nature geoscience
SUPPLEMENTARY INFORMATION
DOI: 10.1038/NGEO2349

Long-term winter warming trend in the Siberian Arctic during the mid- to late Holocene

Hanno Meyer, Thomas Opel, Thomas Laepple, Alexander Yu Dereviagin, Kirstin Hoffmann and Martin Werner

© 2015 Macmillan Publishers Limited. All rights reserved

1 Study region

Figure S1: The study area in the Central Lena Delta. Ice wedges were sampled during field campaigns in 2005 and 2010 in an area of about 30 km around Samoylov Island with its scientific station serving as logistical base.

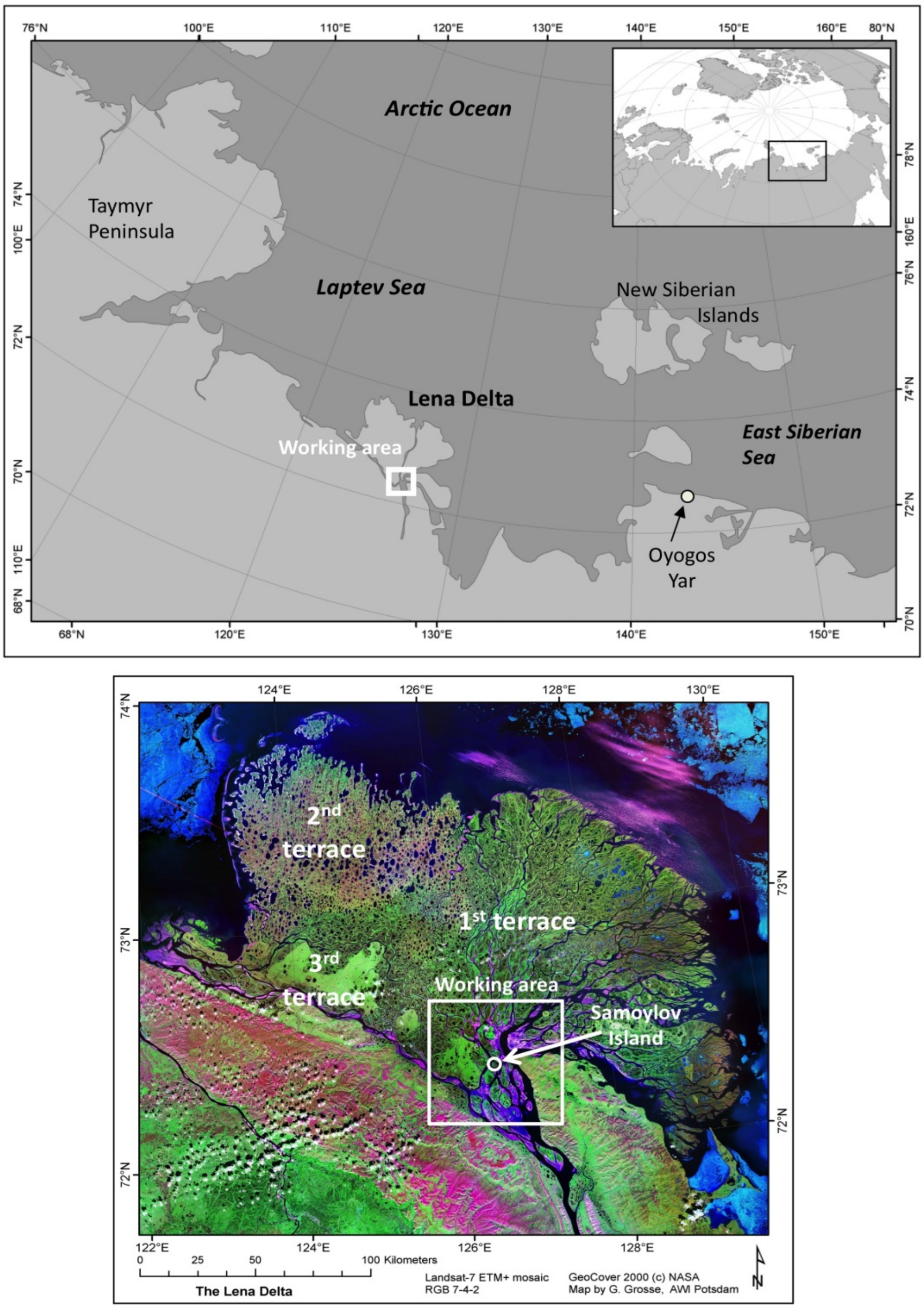

© 2015 Macmillan Publishers Limited. All rights reserved

The study area is situated in the central part of the Lena River Delta (white square; Fig. S1; 72°00’-72°45’N and 125°00’-127°15’E) in Northern Siberia. In this area two (out of three) river terraces were sampled: (1) the first Lena River terrace (dark green colors) comprising the active part of the delta, which was formed from mid Holocene to present. (2) the third Lena River terrace (light green colors), where the work focused on Holocene cover deposits above the Ice Complex with a height of ca. 25 m[1] (Fig S1). In general, the vast landmasses of the Siberian Arctic exhibit permafrost conditions, i.e. defined as ground at or below 0 °C for two or more consecutive years[2]. Ice wedges as one of the most frequent types of permafrost ice are, in general, indicative for cold and stable climate conditions, but may also be developed in interglacial (i.e. Holocene) climate.

2 Stable isotopes in ice wedges

Stable water isotopes were measured with Finnigan MAT Delta-S mass spectrometers at the Alfred Wegener Institute in Potsdam, Germany. Hydrogen and oxygen isotope ratios are given as per mil difference relative to V-SMOW (‰, Vienna Standard Mean Ocean Water), with internal 1σ errors better than 0.8‰ and 0.1‰ for δD and $\delta^{18}O$, respectively[3]. In this paper, $\delta^{18}O$ is interpreted as a proxy for local air temperatures, whereas the *d* excess[4] (*d* excess = $\delta D - 8 * \delta^{18}O$) characterizes sea surface conditions (i.e. relative humidity, temperature) in the moisture source region[5]. In the target season for ice-wedge growth (DJFMAM), precipitation is generally characterized by d excess values of 10‰ and higher[6] (at Zhigansk, Yakutia, near Lena River). A lower *d* excess can be indicative of secondary fractionation processes related to ice-wedge samples with isotopically-altered precipitation involved in the process (sometimes found at the

© 2015 Macmillan Publishers Limited. All rights reserved

lateral contacts with the surrounding sediment), which need to be discarded from climate interpretation[7].

In general, the width of the sampled ice-wedge profiles ranges from 1.0 to 3.5 m depending on the width and shape of each ice wedge exposure and the sampling level. The thickness of single ice veins in Holocene ice wedges varies around a few mm. Accordingly, a single ice-wedge sample of 15 mm width contains approximately 10 ice veins representative of 10 frost cracking events. Taking into account that frost cracking processes forming ice wedges do not occur every year[8], we relate one sample to a period of 20 years. The recent ice wedges (N=12) studied in this paper were taken in 2002, 2005 and 2010 and are thus related to the past 10 years. These show a mean $\delta^{18}O$ value of -22.2‰, which corresponds to the two most recent ^{14}C dated ice-wedge samples (number 1 and 2 in Table S1; $\delta^{18}O$ = -22.5‰; -21.4‰), thus, confirming the recent temperature maximum.

Additionally, system-immanent changes might have an influence on the Lena Delta stable-isotope record. Possible effects are either changes in the seasonality of precipitation, frost cracking and ice-vein formation, isotopic transformation of the snow cover by percolation (either by snow melt or rain water), or hoar frost prior to ice-wedge formation. Furthermore, vegetation changes could potentially alter wind drift properties of a snow cover at a given site. However, in mid to late Holocene times vegetation changes were negligible in our study region, which has been situated north of the treeline during the complete Holocene and has been characterised by wet (shrub) tundra vegetation in mid to late Holocene[9].

© 2015 Macmillan Publishers Limited. All rights reserved

Figure S2: Example of a studied ice wedge (LD05-IW-1; ice-wedge site 1) on Samoylov Island (Fig. S1) with sample positions.

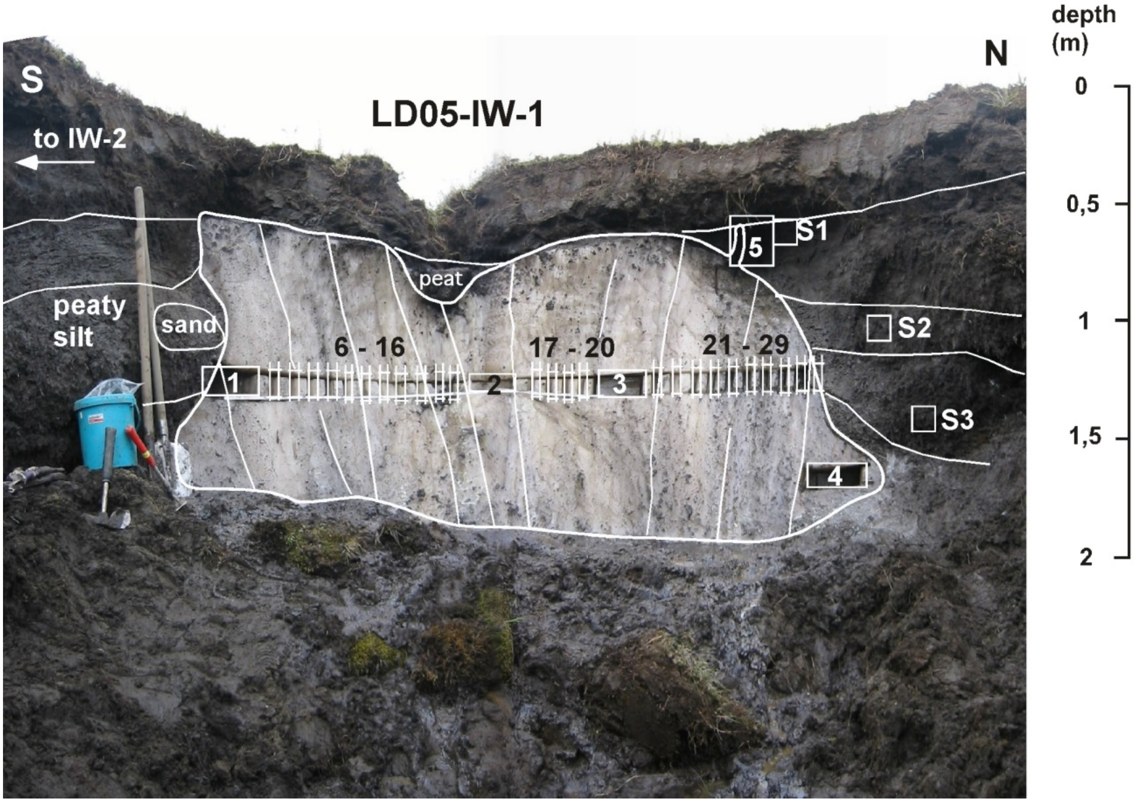

Figure S3: Studied ice wedge (LD05-IW-7; ice-wedge site 4) ca. 30 km NW of Samoylov Island (Fig. S1) with sample positions.

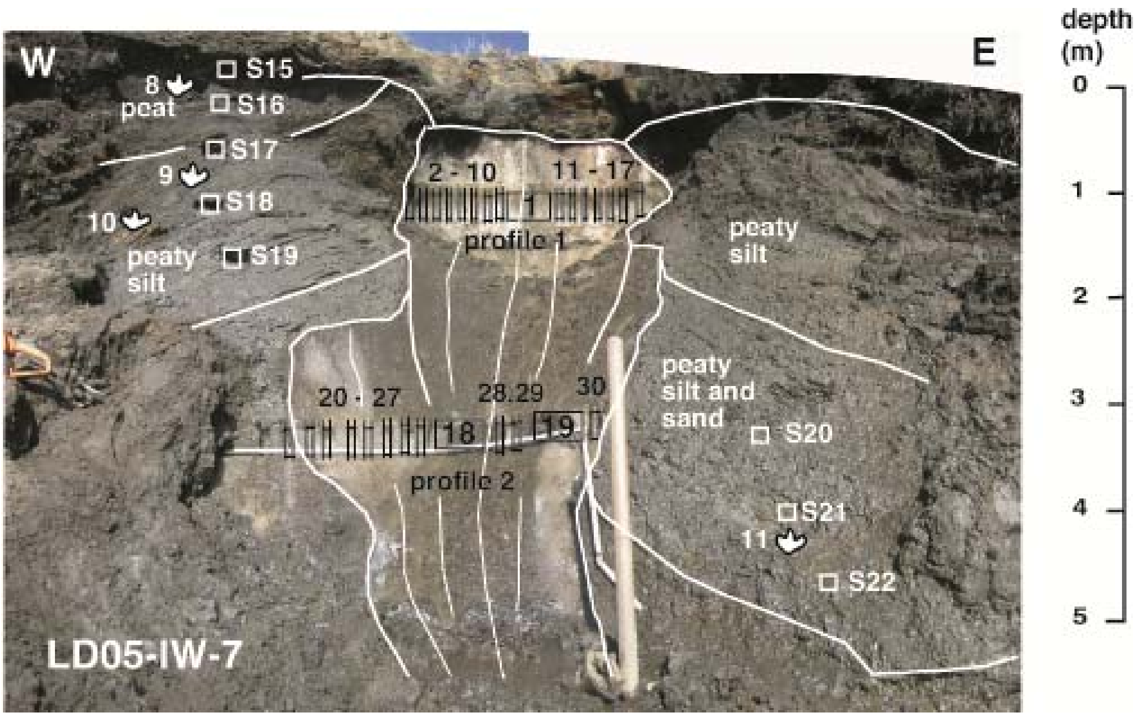

© 2015 Macmillan Publishers Limited. All rights reserved

Figure S4: Example of ice wedge (LD05-IW-8; ice-wedge site 11) ca. 10 km SW of Samoylov Island (Fig. S1) with sample positions.

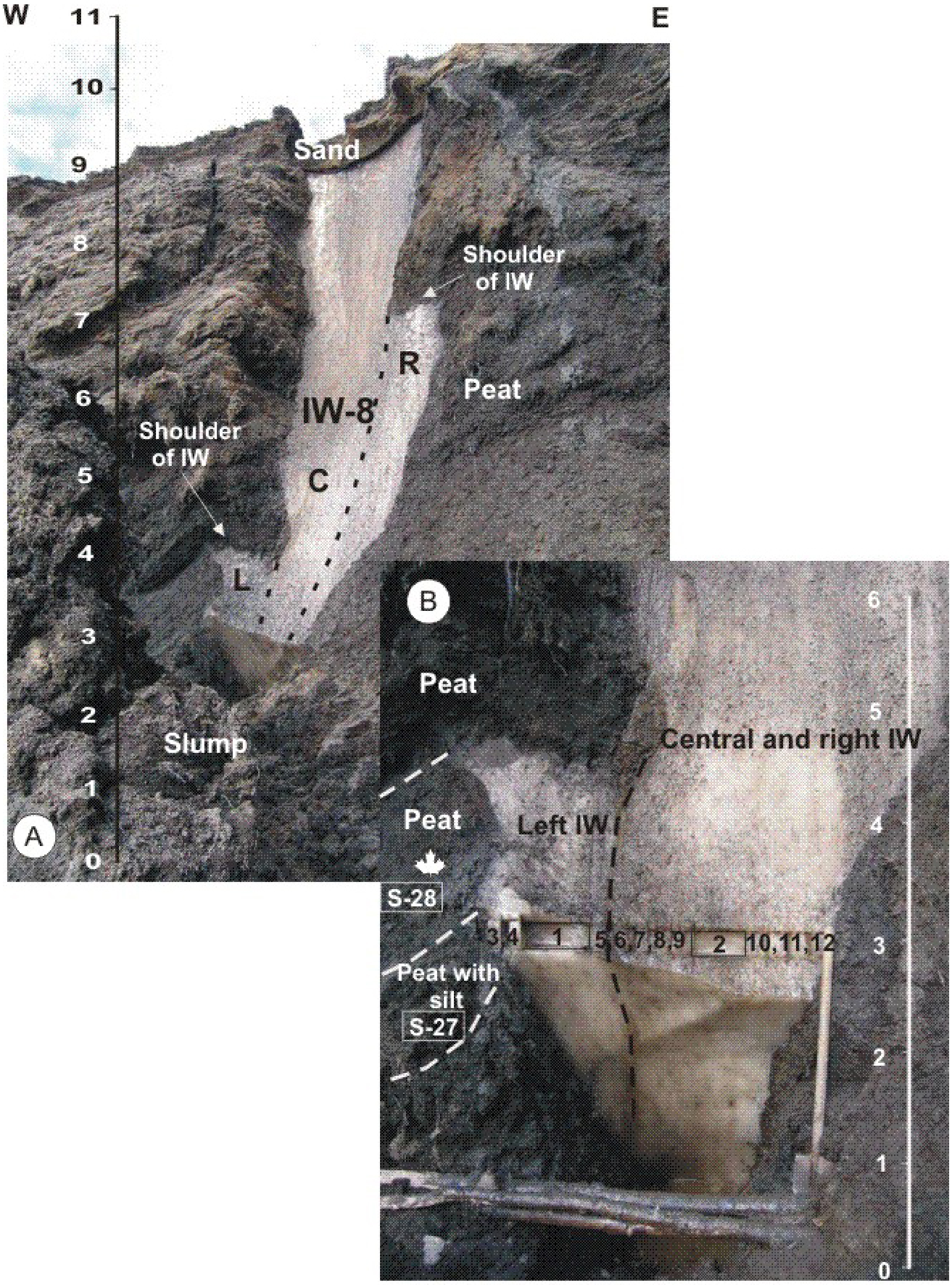

3 Ice-wedge sample selection

The studied ice wedges (see Fig. S2-S4 for the example LD05-IW-1; IW-7 and IW-8) have been sampled by chain saw and slices of about 1.5 cm width were cut out of the

© 2015 Macmillan Publishers Limited. All rights reserved

ice (either in the field or later in the cold laboratory), then melted and analysed for stable O and H isotopes and screened for organic matter content. The studied ice wedges contained organic material (i.e. leaves, twigs, or lemming pellets), which was picked under light microscope for AMS ^{14}C dating.

Out of the 42 samples with sufficient organic matter for dating, 2 samples were excluded from the Lena Delta $\delta^{18}O$ record (see Table S1). Sample number 4 yielded an unusual low *d* excess value of 5.5‰ and has been excluded because secondary fractionation processes (i.e. evaporation of snow melt water) could not be ruled out. Sample number 29 was the only ice-wedge sample from the third terrace (Ice Complex; height ca. 25 m), which contained wood fragments, pointing to redistributed older organic matter and, thus, yielding an unrealistic age.

4 Radiocarbon dating and calibration

Radiocarbon measurements were partly carried out in the AMS facility of the Leibniz Laboratory in Kiel (KIA)[10] as well as in the Cologne AMS facility (COL)[11,12]. In order to eliminate contamination by younger organic acids only the leached residues were used for dating. AMS ^{14}C-ages were calibrated using the tool clam[13] and the IntCal13 calibration curve[14]. For point estimates of ages (used in Table S1, dots in Figs. 1 and 3), we report the highest posterior density region (hpd) with its limits, its midpoint and probability. All hpd ranges add up to 95%. For the analysis of the last 2kyr, we use the full age uncertainty. For modern samples, we assume a normal distribution with parameters estimated from the sampling year and the assumed 20yr integration time of single ice-wedge samples. The distributions are truncated at the sampling year minus

© 2015 Macmillan Publishers Limited. All rights reserved

half the integration time (10 years) and at 1954 AD (the limit given by the bomb ^{14}C). The results are not sensitive to any of these choices (e.g. medians instead of midpoint of the hpd, uniform age distribution for modern samples).

5 Correlation analysis including time uncertainty

To test whether the correlation is robust to the age uncertainty observed in the record and to test, which correlation could be obtained inside the time uncertainty of the radiocarbon dating, we apply the Maximum Covariance test[15]. In this test, the ice wedge record is tuned to the Arctic 2K record by choosing from all 10,000 age-models the one age model, which maximises the correlation.
To test whether this tuned correlation is significant, we generate 10,000 surrogate records of the Arctic 2K record, which have the same autocorrelation as the annual Arctic 2K record. We tune every of these records and note the maximum tuned correlation. Finally, we compare the distribution of maximum correlations obtained from the surrogate data with the maximum correlation based on the proxy records. The maximum correlation of r=0.80 after tuning is significantly higher (p=0.02) than the highest correlation obtained when using tuned surrogate records.

6 Siberian ice wedge isotopes as a temperature proxy

Usually, in high-latitude regions $\delta^{18}O$ variations, e.g. as measured in Greenland ice cores, are regarded as proxy for past temperature changes. However, for any isotope record, e.g. the ice wedge $\delta^{18}O$ record presented in this study, one cannot assume a strong relationship between $\delta^{18}O$ values and local temperatures, a priori. Besides local

© 2015 Macmillan Publishers Limited. All rights reserved

temperatures, several other processes and mechanisms (atmospheric transport, source region changes, seasonality effects, etc.) might influence the $\delta^{18}O$ signal, too. However, several studies, using both observations and isotope modeling results, indicate that temperature is the primary control on $\delta^{18}O$ in the studied Siberian ice wedges.

Modern observations show a strong linear spatial correlation between surface temperatures and isotopes in precipitation (δD_p, $\delta^{18}O_p$) for the Siberian Network of Isotopes in Precipitation (SNIP)[16]. This strong spatial correlation is mainly found in winter (DJF) and can be explained by a classical continental rain-out effect over Siberia, which can be described by a Rayleigh model approach. For summer time, this correlation weakens as re-evaporation and transport of continental water plays a more important role.

Measurements of mean $\delta^{18}O_{ice}$ values of different recent ground ice and ice veins samples from Yakutia also a strong correlation with mean winter temperatures at the sample sites[17].

On the intra-annual temporal scale, observational sites located in proximity of our ice wedge sites (Zhigansk, Olenek, Tiksi) reveal a strong correlation between the seasonal cycle of surface temperatures and $\delta^{18}O_p$[6,16,18].

Simulations with the atmospheric general circulation model ECHAM5-wiso, equipped with stable water isotope diagnostics, also show a strong correlation of the seasonal cycle of surface temperatures and $\delta^{18}O_p$[19]. Furthermore, the model results indicate on the interannual temporal scale a strong correlation of DJF temperatures and $\delta^{18}O_p$ over Siberia for the period 1960-2010, while only a weak or no correlation exists for JJA $\delta^{18}O_p$ values due to an increased influence of regional evaporation and convection

© 2015 Macmillan Publishers Limited. All rights reserved

processes. These ECHAM5-wiso model results are in good agreement with the observational findings by Kurita et al.[16].

For past climate changes, we have analysed modelled temperatures and $\delta^{18}O_p$ values for a suite of different ECHAM5-wiso simulations: a modern control simulation (CNTRL; see Werner et al.,[20] for setup details), simulations under pre-industrial (PI), 5K, and 6K Holocene climate conditions[21], an LGM simulation set up according to the PMIP3 protocol using GLAMAP SST and sea ice boundary conditions, nudged simulations of the years 2001-2010 (PD, see Butzin et al.[19], for setup details), and of the years 2040-2050 assuming an RCP4.5 emission scenario (Butzin, personal communication). The ECHAM5-wiso simulation results might be biased by general model deficits, different simulation modes (free vs. nudged setup) and/or inappropriate boundary conditions for any selected time period. Nevertheless, we rate them as very useful for studying the $\delta^{18}O_p$-T-relation for a potential range of varying climates.

In Fig. S5, we plot simulated precipitation-weighted mean $\delta^{18}O_p$ values versus surface temperature at the Lena Delta ice wedge site for DJF (left) and JJA (right). CNTRL, LGM, PI, 5K, 6K values are based on a single simulation over 10 model years, each. Values for PD and RCP4.5 represent a mean of 3 simulations, each, where nudging fields were derived from 3 different ensemble members of MPI-ESM RCP4.5 simulations performed within the CMIP5 framework. CNTRL, PI, 5K, 6K and LGM simulations have been performed in T106 model resolution. PD and RCP4.5 simulations were run in nudged mode in T63 resolution.

Similar to the present-day situation, a strong correlation (Pearson's linear correlation coefficient $r = 0.97$; Spearman's rank correlation coefficient $\rho = 0.99$) between temperatures and $\delta^{18}O_p$ can be found for the DJF season (Fig. S5, left). A slightly

© 2015 Macmillan Publishers Limited. All rights reserved

weaker correlation ($r = 0.88$; $\rho = 0.83$) is found if the extended "winter" season DJFMAM is considered (not shown). For JJA, variations of temperatures and $\delta^{18}O_p$ are even less correlated ($r = 0.86$; $\rho = 0.71$). The latter might again indicate the stronger influence of regional re-evaporation, transport of continental water, and convection processes, during summer as observed and modelled for the present-day climate[16, 19].

To summarise: Present-day observational data and model results on both spatial and temporal scales as well as our analyses of simulations under different past climate conditions indicate that winter Holocene $\delta^{18}O_p$ values measured in ice wedges have been primarily controlled by local temperature changes. Thus, we interpret the increasing $\delta^{18}O_p$ trend in ice wedges as a winter warming trend during the last 6,000 years, in agreement with the change in incoming solar radiation and increasing GHG forcing.

Figure S5: Simulated mean values of surface temperatures and $\delta^{18}O_p$ in precipitation for the Lena Delta, derived from seven ECHAM5-wiso simulations under different climate boundary conditions (CNTRL, PI, 5K, 6K, LGM, PD, future climate RCP4.5 scenario). Left: winter values (DJF), right: summer values (JJA). The straight lines represent a linear fit through all given data points. Please note the different temperature and $\delta^{18}O$ ranges in the left and right plot.

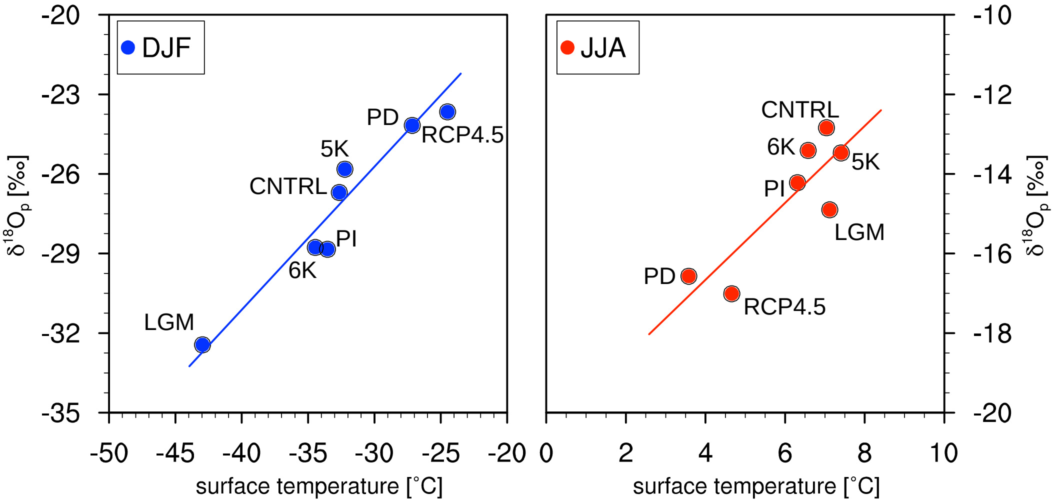

© 2015 Macmillan Publishers Limited. All rights reserved

7 Seasonal temperature change in the PMIP3 simulations

The growth period of ice-wedges (DJFMAM) integrates the classical meteorological seasons winter (DJF) and spring (MAM). To facilitate a comparison with other studies and to investigate the causes for the warming during DJFMAM, we report here the PMIP3 temperature response during the four meteorological seasons (Fig. S6). We analyse the PMIP3 simulations for the study area (72N, 126E), the mid-high latitudinal (30-90N) average covering the same area as reported by Marcott *et al.*[22] (also shown in the main paper, Fig. 2), as well as an Arctic average (60-90N) to allow a comparison with the PMIP1 and PMIP2 model results analysed in Zhang *et al.*[23].

For the geographical position of the ice-wedge records (Lena Delta) as well as for the Arctic region 60-90N, the models show a diverging temperature response for the DJF season. This divergence is likely related to a model-dependent representation of several climatic feedback mechanisms. Whereas the DJF insolation forcing would lead to a winter warming (i.e. 6K colder than PI), ocean, vegetation and sea-ice feedbacks can reverse the impact of the local orbital forcing[23,24] and lead to a winter cooling. It is interesting to note that the model response to DJF insolation forcing seems to be more divergent in the most recent PMIP3 simulations than in the older PMIP2 simulations. For PMIP2, all simulations that included interactive vegetation and most simulations without interactive vegetation show a cooling (i.e. 6K warmer than PI).

In the remaining seasons, simulated temperatures in most PMIP3 models follow more directly the insolation forcing. This leads to a warming in meteorological spring (MAM) and a cooling in summer (JJA) and autumn (SON).

© 2015 Macmillan Publishers Limited. All rights reserved

The mid-high latitude averaged (30-90N) PMIP3 temperature changes, relevant for the comparison with the recent Holocene temperature evolution reconstruction from Marcott *et al.*[22], show an overall similar pattern but a stronger warming and weaker cooling trend. This difference in the amplitude of simulated temperature changes can be attributed to the weaker effect of obliquity changes between 30-60N.

To summarise: the modelled mid-Holocene warming found in the PMIP3 simulations in the Lena Delta during the ice-wedge growth season (DJFMAM) is a combination of a simulated winter (DJF) cooling or warming, which is significantly affected by ocean and land-based climate feedbacks, and a more direct insolation-driven simulated spring (MAM) temperature change.

Figure S6: PMIP3 seasonal 6K-PI temperature changes.
(a) for the Lena Delta area, weighted average of (b) 60-90N and (c) 30-90N. Panel (b) allows a direct comparison with Fig. 3 of Zhang *et al.*[23], which shows the same quantity derived from the PMIP1 and PMIP2 simulations.

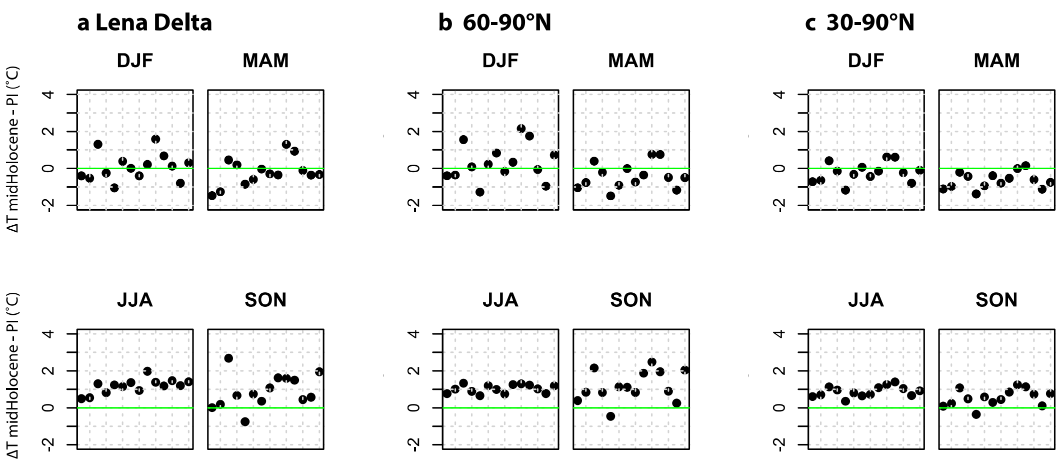

© 2015 Macmillan Publishers Limited. All rights reserved

8 SI References

1 Schwamborn, G., Rachold, V. & Grigoriev, M.N. Late Quaternary sedimentation history of the Lena Delta. *Quat. Intern.* **89**, 119-134, doi:10.1016/S1040-6182(01)00084-2 (2002).

2 van Everdingen, 2005 Multi-language Glossary of Permafrost and Related Ground-Ice Terms (International Permafrost Association, 1998).

3 Meyer, H., Schoenicke, L., Wand, U., Hubberten, H.-W. & Friedrichsen, H. Isotope studies of hydrogen and oxygen in ground ice - Experiences with the equilibration technique. *Isot. Environ. Health Stud.* **36,** 133-149, doi:10.1080/10256010008032939 (2000).

4 Dansgaard, W. Stable isotopes in precipitation. *Tellus* **16**, 436-468 (1964).

5 Merlivat, L. & Jouzel, J. Global climatic interpretation of the deuterium-oxygen 18 relationship for precipitation. *J. Geophys. Res.* **84,** 5029-5033 (1979).

6 Kurita, N. Origin of Arctic water vapor during the ice-growth season. *Geophys. Res. Lett.* **38**, L02709, doi:10.1029/2010GL046064 (2011).

7 Meyer, H., Dereviagin, A.Y., Siegert, C., Schirrmeister, L. & Hubberten, H.-W. Paleoclimate reconstruction on Big Lyakhovsky Island, North Siberia. – Hydrogen and oxygen isotopes in ice wedges. *Permafrost and Periglacial Processes* **13**, 91-105 (2002).

8 Mackay, J. R. Oxygen isotope variations in permafrost, Tuktoyaktuk Peninsula area, Northwest Territories. *Current Research, Part B, Geological Survey of Canada* Paper **83-1B,** 67-74 (1983).

9 Wetterich, S. *et al.* Palaeoenvironmental dynamics inferred from late Quaternary permafrost deposits on Kurungnakh Island, Lena Delta, Northeast Siberia, Russia. *Quat. Sci. Rev.* **27**, 1523-1540, doi:10.1016/J.Quascirev.2008.04.007 (2008).

© 2015 Macmillan Publishers Limited. All rights reserved

10 Nadeau, M. J. *et al*. The Leibniz-Labor AMS facility at the Christian-Albrechts University, Kiel, Germany. *Nuclear Instruments & Methods in Physics Research Section B* **123,** 22-30, doi:10.1016/s0168-583x(96)00730-6 (1997).

11 Dewald, A. *et al.* CologneAMS, a dedicated center for accelerator mass spectrometry in Germany. *Nuclear Instruments & Methods in Physics Research Section B* **294,** 18-23, doi:10.1016/j.nimb.2012.04.030 (2013).

12 Rethemeyer, J. *et al.* Status report on sample preparation facilities for C-14 analysis at the new CologneAMS center. *Nuclear Instruments & Methods in Physics Research Section B* **294,** 168-172, doi:10.1016/j.nimb.2012.02.012 (2013).

13 Blaauw, M. Methods and code for 'classical' age-modelling of radiocarbon sequences. *Quat. Geochronol.* **5,** 512-518. doi:10.1016/j.quageo.2010.01.002 (2010).

14 Reimer, P.J. *et al.* IntCal13 and Marine13 radiocarbon age calibration curves 0–50,000 years cal BP. *Radiocarbon* 55(4), 1869-1887 (2013).

15 Haam, E., & Huybers, P. A test for the presence of covariance between time-uncertain series of data with application to the Dongge Cave speleothem and atmospheric radiocarbon records. *Paleoceanography* **25,** PA2209, doi:201010.1029/2008PA001713 (2010).

16 Kurita, N., Yoshida, N., Inoue, G. & Chayanova, E.A. Modern isotope climatology of Russia: A first assessment. *J. Geophys. Res.* **109**, D03102. doi:10.1029/2003jd003404 (2004).

17 Nikolayev, V.I. & Mikhalev, D.V. An Oxygen-Isotope Paleothermometer from Ice in Siberian Permafrost. *Quat. Res.* **43**, 14–21. doi:10.1006/qres.1995.1002 (1995).

© 2015 Macmillan Publishers Limited. All rights reserved

18 Kloss, A.L. Water isotope geochemistry of recent precipitation in Central and North Siberia as a proxy for the local and regional climate system. Diploma thesis. Leibniz University, Hannover (2008).

19 Butzin, M. *et al.* Variations of oxygen-18 in West Siberian precipitation during the last 50 years. *Atmospheric Chemistry and Physics* **14**, 5853–5869. doi:10.5194/acp-14-5853-2014. (2014).

20 Werner, M., Langebroek, P.M., Carlsen, T., Herold, M. & Lohmann, G. Stable water isotopes in the ECHAM5 general circulation model: Toward high-resolution isotope modeling on a global scale. *J. Geophys. Res*. doi:10.1029/2011jd015681 (2011).

21 Dietrich, S., Werner, M., Spangehl, T. & Lohmann, G. Influence of orbital forcing and solar activity on water isotopes in precipitation during the mid- and late Holocene. *Clim. Past* **9**, 13–26. doi:10.5194/cp-9-13-2013 (2013).

22 Marcott, S.A., Shakun, J.D., Clark, P.U. & Mix, A.C. A Reconstruction of Regional and Global Temperature for the Past 11,300 Years. *Science* **339**, 1198-1201, doi:10.1126/science.1228026 (2013).

23 Zhang, Q. *et al.* Climate change between the mid and late Holocene in northern high latitudes; Part 2: Model-data comparisons. *Clim. Past* **6**, 609-626, doi:10.5194/cp-6-609-2010 (2010).

24 Wohlfahrt, J., Harrison, S. P. & Braconnot, P. Synergistic Feedbacks between Ocean and Vegetation on Mid- and High-Latitude Climates during the Mid-Holocene. *Clim. Dyn.* **22**(2-3), 223-238, doi:10.1007/s00382-003-0379-4 (2004).

© 2015 Macmillan Publishers Limited. All rights reserved

Table S1: Radiocarbon dates of organic matter from Lena Delta ice wedges dated in Kiel (KIA) and Cologne (COL) radiocarbon laboratories. All samples have been calibrated with the tool clam[12] using INTCAL13 and are given in yr cal b2K (before AD 2000)[13] midpoint, range and probability of the highest posterior density (hpd). Additionally, $\delta^{18}O$ values of every ice-wedge sample, the respective sedimentary unit and sampled organic matter are given. Two $\delta^{18}O$ values (marked with brackets) have been excluded from the stacked isotope record (for further details, see SI).

No	Sample ID	Ice wedge site	Lab ID	Radiocarbon age	Error	Calibrated age midpoint of hpd	range of hpd	Probability	$\delta^{18}O$	Unit	Material
				[yr BP]	±	[yr cal b2K]	[± yr]	[%]	[‰; V-SMOW]		
1	LD05-IW-1.16	1	KIA33163	> 1954 AD	0	**25**	10	NA	-22.46	Lena river terrace	lemming pellet
2	LD10-IW-13.13	2	COL1725	> 1954 AD	0	**23**	10	NA	-21.26	Top Ice Complex	plant remains
3	LD05-IW-11.10	3	KIA29851	220	25	**218**	20	40.3	-24.95	Top Ice Complex	plant remains
4	LD05-IW-7.11	4	KIA29847	183	42	**230**	50	47.0	(-22.76)	Lena river terrace	peat
5	LD05-IW-12.19	5	KIA29852	297	39	**429**	91	95.0	-24.90	Lena river terrace	peat
6	LD05-IW-7.1-I15/16	4	COL1067	287	34	**454**	56	62.1	-24.04	Lena river terrace	sphagnum, wood
7	LD05-IW-1.2-I5	1	COL1061	388	53	**516**	48	54.0	-23.55	Lena river terrace	sphagnum, leaves
8	LD10-IW-15.15	6	COL1351	389	30	**518**	41	68.6	-24.85	Lena river terrace	plant remains
9	LD05-IW-1.18	1	KIA33162	416	31	**527**	44	85.0	-24.20	Lena river terrace	plant remains
10	LD05-IW-1.20	1	KIA33161	834	36	**789**	57	92.2	-23.90	Lena river terrace	plant remains
11	LD05-IW-10.8	7	KIA29850	965	26	**885**	39	59.9	-23.59	Lena river terrace	peat
12	LD05-IW-9.12	8	KIA33167	1011	24	**988**	30	92.2	-23.42	Lena river terrace	plant remains
13	LD05-IW-5.4-I10/11	9	COL1066	1060	38	**1019**	44	75.7	-25.31	Lena river terrace	sphagnum
14	LD05-IW-10.14	7	KIA33169	1105	26	**1060**	52	95.0	-23.43	Lena river terrace	plant remains
15	LD05-IW-7.29	4	KIA36116	1075	74	**1089**	139	88.6	-24.51	Lena river terrace	plant remains
16	LD05-IW-13.9	10	KIA36120	1159	70	**1120**	117	85.2	-25.11	Lena river terrace	plant remains
17	LD05-IW-1.4-I2	1	COL1062	1164	34	**1160**	68	73.9	-24.89	Lena river terrace	sphagnum
18	LD05-IW-1.11	1	KIA29843	1307	30	**1308**	34	66.5	-23.87	Lena river terrace	plant remains

© 2015 Macmillan Publishers Limited. All rights reserved

19	LD05-IW-5.12	9	KIA36114	1405	66	**1370**	95	88.9	-24.14	Lena river terrace	plant remains
20	LD05-IW-12.9	5	KIA36119	1561	35	**1506**	77	95.0	-25.04	Lena river terrace	plant remains
21	LD05-IW-1.21	1	COL1345	1676	72	**1621**	167	94.2	-23.47	Lena river terrace	plant remains
22	LD05-IW-9.6	8	KIA33166	1666	34	**1625**	54	84.9	-23.52	Lena river terrace	plant remains
23	LD10-IW-15.2	6	COL1726	1689	46	**1667**	95	93.9	-25.49	Lena river terrace	plant remains
24	LD05-IW-5.1-I8+I9	9	COL1064	1739	37	**1692**	87	95.0	-24.45	Lena river terrace	sphagnum
25	LD05-IW-7.23	4	KIA36115	1749	67	**1728**	146	95.0	-24.93	Lena river terrace	plant remains
26	LD05-IW-1.27	1	KIA36113	2019	38	**2024**	88	92.4	-23.44	Lena river terrace	plant remains
27	LD05-IW-7.15	4	COL1731	2053	42	**2074**	101	93.6	-24.45	Lena river terrace	plant remains
28	LD05-IW-9.4	8	KIA29849	2080	33	**2114**	78	92.5	-24.87	Lena river terrace	peat
29	LD10-IW-13.9	2	COL1350	2083	32	**2116**	78	94.1	(-21.04)	Top Ice Complex	plant remains, wood
30	LD05-IW-1.22	1	KIA29844	2126	95	**2178**	205	94.2	-23.04	Lena river terrace	peat
31	LD05-IW-1.3-I5	1	COL1730	2201	44	**2275**	108	95.0	-23.58	Lena river terrace	plant remains
32	LD05-IW-12.5	5	KIA33168	2623	28	**2804**	24	95.0	-25.27	Lena river terrace	plant remains
33	LD05-IW-5.13	9	KIA33164	3000	62	**3228**	174	95.0	-24.93	Lena river terrace	peat
34	LD05-IW-11.5	3	KIA36118	3014	35	**3252**	67	69.4	-25.85	Top Ice Complex	plant remains
35	LD05-IW-5.16	9	KIA29845	3630	84	**3980**	225	94.5	-24.81	Lena river terrace	peat
36	LD05-IW-8.6	11	KIA29848	4107	41	**4674**	104	69.9	-25.98	Lena river terrace	peat
37	LD05-IW-8.7	11	KIA36117	5178	33	**5996**	47	95.0	-25.88	Lena river terrace	plant remains
38	LD05-IW-8.1-I11/12	11	COL1068	5211	42	**6014**	60	83.1	-26.53	Lena river terrace	sphagnum
39	LD05-IW-8.2-AK2	11	COL1069	5273	38	**6104**	74	64.8	-28.18	Lena river terrace	wood
40	LD05-IW-8.9	11	KIA33165	5332	44	**6154**	110	89.9	-26.76	Lena river terrace	plant remains
41	LD10-IW-12.29	12	COL1724	5437	50	**6296**	71	87.6	-25.26	Top Ice Complex	plant remains
42	LD05-IW-3-I33	13	COL1063	6336	44	**7300**	82	87.4	-25.82	Lena river terrace	sphagnum

© 2015 Macmillan Publishers Limited. All rights reserved

Table S2: PMIP3 models analysed in this study.

model name	#ensemble members	institute/research group
BCC-CSM1.1	1	Beijing Climate Center, China Meteorological Administration
CCSM4	2	National Center for Atmospheric Research
CNRM-CM5	1	Centre National de Recherches Metéorologiques/Centre Européen de Recherche et de Formation
CSIRO-Mk3-6-0	1	CSIRO (Commonwealth Scientific and Industrial Research Organisation, Australia), and BOM (Bureau of Meteorology, Australia)
GISS-E2-R	1	NASA Goddard Institute for Space Studies
HadGEM2-CC	1	Met Office Hadley Centre
HadGEM2-ES	1	Met Office Hadley Centre
IPSL-CM5A-LR	1	Institut Pierre-Simon Laplace
MPI-ESM-P	1	Max-Planck-Institut für Meteorologie
MRI-CGCM3	1	Meteorological Research Institute
FGOALS-g2	1	LASG, Institute of Atmospheric Physics, CAS and CESS Tsinghua University
FGOALS-s2	1	LASG, Institute of Atmospheric Physics, CAS and CESS Tsinghua University
MIROC-ESM	1	Atmosphere and Ocean Research Institute (The University of Tokyo), National Institute for Environmental Studies, and Japan Agency for Marine-Earth Science and Technology

© 2015 Macmillan Publishers Limited. All rights reserved